Engineering magnetic type radio-absorbers based on composites with a dual-phase polymer matrix

Engineering Magnetic Type Radio-Absorbers Based on Composites with a Dual-Phase Polymer Matrix

Marek Gořalík[1], Marek Jurča[2], Constantin Bubulinca[2], Vladimír A. Babayan[2], Jarmila Vilčáková[1,2], Natalia E. Kazantseva[1,2], Petr Sáha[1,2]

[1]Polymer Centre, Faculty of Technology, Tomas Bata University in Zlin, nám. T. G. Masaryka 5555, 76001 Zlín, Czech Republic

[2]Centre of Polymer Systems, University Institute, Tomas Bata University in Zlin, nám. T. G. Masaryka 5555, 76001 Zlín, Czech Republic

[*]Jarmila Vilčáková vilcakova@utb.cz

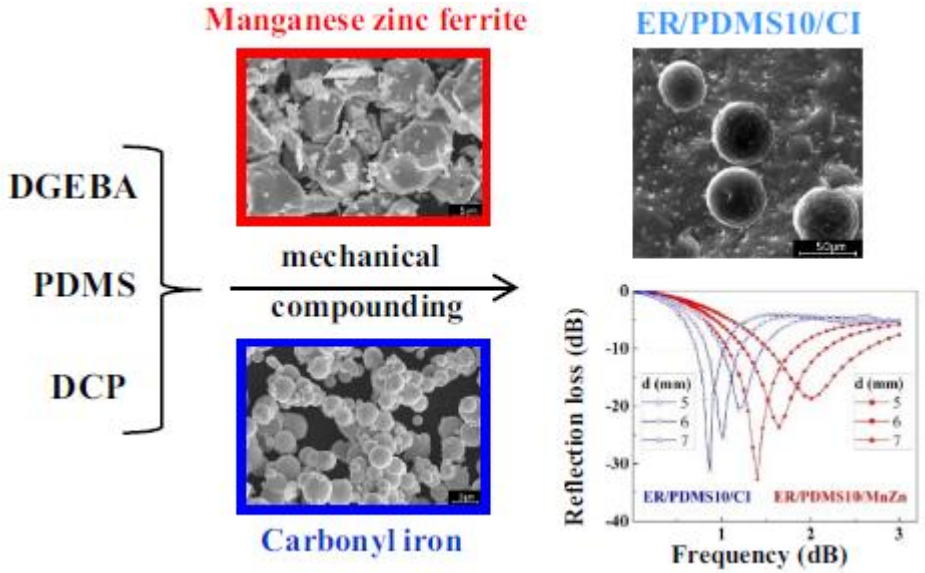

Abstract

This work is focused on the optimization of electromagnetic and mechanical properties of magnetic polymer composites for EMI applications as radio absorbers (RAs). Polymer composites with a dual-phase polymer matrix, vinyl-terminated poly-dimethylsiloxane (PDMS) in epoxy (ER), were investigated for fabricating highlyfilled manganese zinc ferrite (MnZn) and carbonyl iron (CI) composites with respect to radio-absorption and mechanical properties. The dielectric and magnetic properties of the composites were determined by the type, concentration as well as the polymer matrix composition. Increase of the filler and the PDMS concentration leads to an increase in magnetic losses due to a decrease in the demagnetizing field. The electromagnetic properties of the composites were evaluated in the RF band using the impedance method (1 MHz-3 GHz). Based on the complex permittivity (ε^*) and the complex permeability (μ^*), the reflection loss RL (dB) of single-layer metal-backed RAs were calculated. The RAs with a MnZn ferrite demonstrated a larger bandwidth to thickness ratio in comparison with the CI-based RAs due to a proper ratio between ε^* and μ^* which leads to the better impedance matching conditions. According to the mechanical analyses (DMA, Charpy impact strength) the significant increase of stiffness up to 125% and the impact strength up to 150% was achieved due to the optimal composition of the polymer matrix and the filler.

Keywords: Radio absorber, reflection loss, electromagnetic properties, magnetic polymer composites, polymer blends

Introduction

There is a growing use of radio-absorbers (RAs) in commercial electronics which is associated with a necessity to reduce the interference of electromagnetic waves inside houses (office, laboratory etc.), aircraft cabin and also to protect human beings. High-frequency wireless devices often have powerful transmitters and sensitive receivers in close proximity. Spurious signals can cause leakage or system interference which degrades network servers. The frequency range 0.8-12 GHz is of particular importance here as the majority of communication and information transfer systems operate in this frequency region.

This has resulted in intensive research in the field of RAs for their use in minimizing the harmful effects of electromagnetic (EM) waves on biological tissues as well as in the form of electromagnetic interference EMI [**1, 2**]. As the name implies, RA reduces the reflection of incident electromagnetic waves through dielectric and/or magnetic losses and represents a layer (layers) of a radio-absorbing material (RAM) placed on a higly-conductive surface. For polymer composites-based EMI shielding materials, a desirable EMI was often achieved via the high loading of conductive fillers or a large coating thickness, which unavoidably caused an increase in the weight of resultant polymer composites [**3**]. The standard objective of the design of RAs is to obtain an absorber of minimal thickness which has the lowest possible reflectance within the widest possible operating bandwidth (bandwidth with the reflection coefficient $R \leq 10$ dB). To optimize the use of the RAs in a design, there are sets of parameters which should be taken into account simultaneously: electromagnetic, mechanical and application. From the point of view of electrodynamics, a more efficient absorption of electromagnetic radiation can be achieved by using RAMs with high permeability, high magnetic loss, a favorable form of frequency dependence of complex permeability (μ^*) and complex permittivity (ε^*) and a proper ratio between the permeability and the permittivity in a certain frequency range [**4**]. The physical performance guidelines are implied by the mechanical properties, the environmental resistance and the lifespan of RAMs. The application dictates the RA type and the choice of materials and technology for its design. Common RAMs used for RAs are plastics, elastomers as well as composites containing conductive and magnetic fillers [**5**]. Any RA operates in a limited operating frequency band. The usual method for expanding the operating frequency band of an RA consists of using multilayer structures (such as gradient index materials) instead of single-layer ones (the Dallenbubach screen) [**6**]. However, this increases the thickness and the weight of the RAs and moreover the design of multilayer absorbers may be very sensitive to the material parameters in each layer. Thus, designing and fabricating single-layer magnetic type RAs are still now preferable [**7, 8**].

Currently, there is a tendency to use nanomaterials for fabricating RAs regardless of the fact that it is a time-consuming and costly process which imposes restrictions for scale production [**9**]. The common technology for RAMs preparation remains as mixing polymers with micron-sized magnetic and/or electrically-conductive fillers [**10, 11**].

The absorption of electromagnetic waves in RAMs is governed by various loss mechanisms related to the magnetization and electric polarization processes [**12**]. Taking into account the fact that the frequency dispersion of μ^* and ε^* in these materials is structure-sensitive, one can manipulate the electromagnetic absorbing properties of a material over a wide frequency range by changing the structural-morphological properties of the filler, the volume fraction of the filler, and the microstructure of the composite. Processing the polymeric composites utilizes different techniques,

however more often it is compression moulding due to the simplicity of the operation and capability regarding the polymer matrix selection [**5**]. The primary function of the polymer in the composites is to bind the filler particles together and insure the physical-and-mechanical properties. At the same time, depending on the filler type, the polymer can reduce the eddy current losses, and, facilitate the non-uniform magnetic flux distribution over the enclosed volume, thereby affecting the internal demagnetizing field [**13**]. Consequently, it results in a decrease in μ^* and an uncontrolled variation of complex permeability as a function of the frequency [**14-16**].

In our previous work, we showed that using immiscible polymer blends based on epoxy resin (ER) and various types of polydimethylsiloxanes (PDMS) for preparing filled composites can affect not only the mechanical but also the electrical properties [**17, 18**]. The change in the electrical properties of composites is associated with the clustering of conducting particles at the ER/PDMS interface, which leads to a decrease in the percolation threshold and an increase in the dc conductivity. The ability of the particles to form a cluster at the interface between two immiscible polymers was used in this work to minimize the internal demagnetizing fields in the magnetic composites and thus increase the efficiency of the single-layer RAs in terms of the reflection coefficient and the operating frequency band. An additional purpose of the work was to improve the RA mechanical properties. To this end, the proper choice of polymer matrix composition, type of magnetic filler and its concentration, as well as optimization of composites technology was performed.

2 Experimental

2.1 Fillers

Two types of commercially available magnetic filler, manganese-zinc (MnZn) ferrite and carbonyl iron (CI) were selected due to their high magnetization saturation and strong electromagnetic energy absorption capacity [**19, 20**].

(i) Sintered MnZn ferrite purchased from "Ferropribor" (St. Petersburg, RF). According to the product information, MnZn ferrite exibites the following properties: initial permeability μ_i = 3000-5000; maximum magnetic permeability $\mu_{max} \sim$ 3700-5200, DC conductivity σ_{DC} = 2 x 10^{-2} S-cm^{-1}, and a density ρ=4 0.8 g-cm^{-3}. Sintered MnZn cores were crushed into smaller pieces and then were mechanically ground by a ball mill (Laarmann Lab Wizz LMLW-320/2, Germany) to obtain ferrite micron-sized particles. The acquired ferrite powder was separated into several batches using a set of sieves so that the particle size distribution was controlled to be between 45 μm and 50 μm.

(ii) The CI of SL type (BASF company, Germany) was used in this study. It is spherical iron particles ($\pm$ 98% aFe) with particle size of about 9 pm and a density ρ = 7 0.8 g-cm^{-3}. This type of CI is characterized by a polycrystalline structure, and a higher value of ε^* and μ^* in the RF region compared to CI with an onion-like structure, such as ES and HQ [**19**].

2.2 Polymers

The polymer matrix of composites was made from two components:

(i) Epoxy resin bisphenol A diglycidyl ether (DGEBA, D-3415, epoxide equivalent weight = 172-176 g, liquid, Sigma Aldrich, USA). The curing agent was an aliphatic amine, i.e. diethylenetriamine (DETA-D93856, Sigma Aldrich, USA).

(ii) Vinylterminated polydimethylsiloxane (PDMS), liquid, Dicumyl peroxide (DCP), free radical initiator

All chemicals were purchased from Sigma Aldrich (USA) with a purity of >90%.

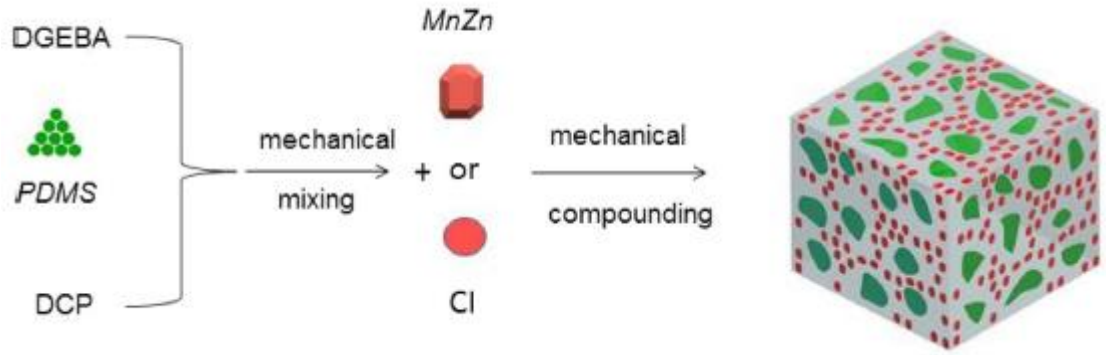

Fig. 1 Schematic illustration of the magnetic composite preparation

2.3 Preparation of the Composites

The first step, an immisible polymer blend of DGEBA, PDMS (10-30 wt.%) and DCP (0.5 wt.%) was prepared under mechanical stirring (MM-1000, Biosan, Germany) at 300 rpm under a nitrogen atmosphere for 2 h at 130 °C. Then, the blend obtained was loaded with a magnetic filler (CI or MnZn ferrite) and stirred at 80 °C for 30 min. The concentration of the filler in the blend varied from 50 wt.% up to 80 wt.%. The equimolar amount of the DETA curing agent was added to the mixture after 10 min before casting the composition onto a preheated to 70 °C mold. The curing process was performed at 100 °C for 30 min and 1 h at 140 °C. **Figure 1** shows the schematic illustration of the magnetic composites fabrication process. The phase composition and the DC conductivity of the composites obtained are listed in **Table 1**.

3 Characterizations

3.1 Scanning Electron Microscopy

To investigate the phase morphology of the epoxy-polydimethylsiloxane/magnetic composites, a VEGA//LMU Tes-can scanning electron microscopy (SEM) was used. The SEM images were obtained under conventional secondary electron imaging conditions with an acceleration voltage of 25 kV and a resolution of 3 nm at 30 kV.

3.2 X-ray Photoelectron Spectroscopy (XPS)

The X-ray photoelectron spectroscopy (XPS) signals were recorded using a Thermo Scientific K-AlphaXPS system (Thermo Fisher Scientific, UK) equipped with a micro-focused monochromatic Al Kα X-ray source (1486.68 eV).

Table 1 The DC conductivity and the impact strength of the polymer magnetic composites

Composites	DC conductivity (S/m)	Impact strength (kJ/m^2)
ER/MnZn50	$(1.22 \pm 0.12) \times 10^{-7}$	20.75 ± 0.01
ER/MnZn70	$(1.15 \pm 0.10) \times 10^{-6}$	11.35 ± 0.03
ER/MnZn80	$(2.81 \pm 0.10) \times 10^{-6}$	8.61 ± 0.02
ER/PDMS10/MnZn50	$(4.41 \pm 0.12) \times 10^{-7}$	15.35 ± 0.01
ER/PDMS10/MnZn70	$(1.07 \pm 0.11) \times 10^{-5}$	9.47 ± 0.02
ER/PDMS10/MnZn80	$(4.62 \pm 0.15) \times 10^{-7}$	7.43 ± 0.02
ER/PDMS30/MnZn50	$(1.27 \pm 0.13) \times 10^{-6}$	14.82 ± 0.04
ER/PDMS30/MnZn70	$(4.12 \pm 0.12) \times 10^{-8}$	11.77 ± 0.03
ER/PDMS30/MnZn80	$(1.16 \pm 0.15) \times 10^{-6}$	11.21 ± 0.01
ER/CI50	$(5.49 \pm 0.10) \times 10^{-8}$	20.75 ± 0.02
ER/CI70	$(5.79 \pm 0.11) \times 10^{-7}$	11.35 ± 0.04
ER/CI80	$(2.74 \pm 0.11) \times 10^{-6}$	8.62 ± 0.03
ER/PDMS10/CI50	$(8.16 \pm 0.15) \times 10^{-8}$	15.36 ± 0.03
ER/PDMS10/CI70	$(4.86 \pm 0.10) \times 10^{-7}$	9.44 ± 0.02
ER/PDMS10/CI80	$(2.85 \pm 0.15) \times 10^{-7}$	7.41 ± 0.01
ER/PDMS30/CI50	$(2.13 \pm 0.13) \times 10^{-7}$	14.83 ± 0.02
ER/PDMS30/CI70	$(2.26 \pm 0.15) \times 10^{-7}$	11.75 ± 0.03
ER/PDMS30/CI80	$(1.35 \pm 0.12) \times 10^{-6}$	11.34 ± 0.01

An X-ray beam of 400 µm in size was used at 6 mA and 12 kV. The spectra were acquired in the constant analyser energy mode with a pass energy of 200 eV for the survey. The narrow regions were collected with a pass energy of 50 eV. The charge compensation was achieved with the system flood gun. The Version 5.9199 (Thermo Fisher Scientific) was used for digital acquisition and data processing. The spectral calibration was determined using the automated calibration routine and the internal Au, Ag and Cu standards supplied with the K-Alpha system.

3.3 DC Conductivity

The DC conductivity was measured by a four-point van der Pauw method (Keithley 6517A, USA) as a current meter and a Multimeter (Keithley 2410, USA) as a source and [**21**].

3.4 Magnetic and Dielectric Spectra

The electromagnetic properties of the composites (ε^* and μ^*) in an RF range from 1 MHz to 3 GHz were measured by the impedance method using (Impedance/Material Analyser E4991A, Agilent Technologies Limited USA). The dielectric spectra were measured on the circular samples with a diameter of 15 mm and the magnetic spectra were measured on the toroidal samples with an outer diameter of 8 mm and an inner diameter of 3.1 mm and 2 mm thickenss.

3.5 Dynamical Mechanical Analysis

The dynamical mechanical analysis (DMA) were carried out under dual cantilever geometry in dynamic (frequency/strain experiments) on a Mettler Toledo DMA1 dynamic mechanical thermal analyzer (DMTA) equipped with a liquid-nitrogen apparatus operating in a three-point bending mode. The tested samples had a dimension of 35 x 10 x 3 mm. The dynamic analysis was carried out from - 120 °C to 180 °C at a heating rate of 3 °C/min, with a fixed frequency of 1 Hz and an amplitude of 20 μm.

3.6 Charpy Impact Strength

The Charpy impact tests were performed in accordance with ISO 179 on unnotched izod specimens using an impact tester (Zwick/Roell, Germany). The dimensions of the samples were 35 x 10 x 3 mm. The fracture mechanism of the polymer systems was studied on the surface of the fractured area via SEM. The mean values over five specimens are presented.

4 Electromagnetic Wave Absorption Evaluation

4.1 Reflection Coefficient: Calculation Technique

For a single-layer metal-backed RA (**Fig. 2**), the absorption of electromagnetic energy is a function of frequency. Based on a generalized transmission line theory, the reflection loss (RL) can be evaluated from the measured magnetic and dielectric spectra and the RA thickness by the following equations:

$$\mathrm{RL} = 20 \log \left| \frac{\mathrm{Z} - \mathrm{Z}_0}{\mathrm{Z} + \mathrm{Z}_0} \right| \qquad (1)$$

in which the normalized input impedance can be computed according to the transmission-line theory. To satisfy the minimum reflection loss, according to **Eq. 1** the perfect matching conditon is,

$$Z = j\sqrt{\frac{\mu}{\varepsilon}} \tan\left(\frac{2\pi f}{c}\sqrt{\mu^*\varepsilon^*}d\right) \qquad (2)$$

Z is the input impedance of the layer, Z_0 is the wave impedance of the free space; f is the frequency; c is the velocity of the light; d is the layer thickess; ε^* and μ^* are complex relative permittivity and permeability.

If the condition Z = 1 is fulfilled, the reflection from the RA is absent. To find these conditions in RAMs a numerical procedure close to a graphical procedure is usually applied to find the mathing frequency f_0 and the mathing thickness d_0 [**15**].

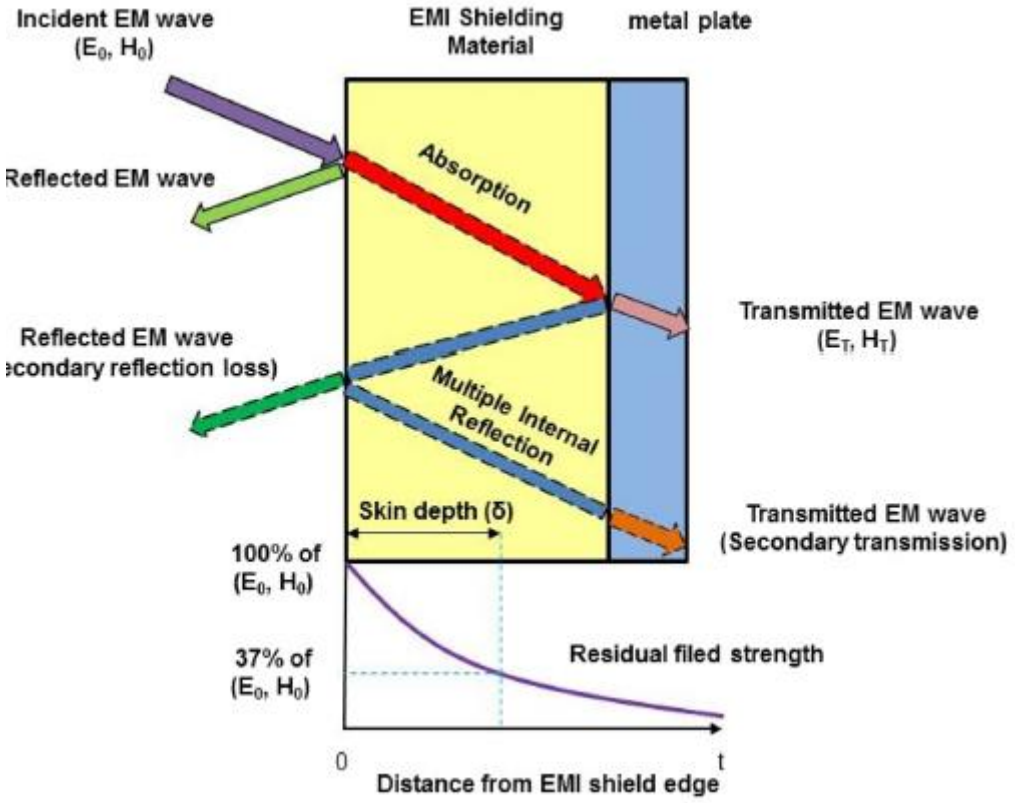

Fig. 2 Schematic representation of a single-layer metal-backed RA

The complex permittivity (ε'and ε'') and the complex permeability (μ'and μ'') are important EM parameters for evaluating the microwave absorption performance. The ε'and ε''are related to the dielectric properties, and the μ'and μ''are associated with the magnetic properties [**22**].

From **Eqs.** (**1**) and (**2**)

$$d = d' + jd'' = \frac{c}{2\pi\sqrt{\mu^*\varepsilon^*}} \arctan\left(-j\sqrt{\frac{\mu^*}{\varepsilon^*}}\right) \qquad (3)$$

Then, Eq. (**3**) was used to calculate the dependence of the complex parameter d on the frequency f and to find the minima of the ratio $\left|\frac{d''}{d'}\right|$ from the obtained curve. Then, the minima for which $\left|\frac{\partial''}{d}\right|$ $\leq$ 0.01 are selected and the thicknesses d_0=d' corresponding to these minima are determined. For the selected values of the parameter d0, the frequency characteristics of the reflection loss are calculated with **Eqs**. (**1**) and (**2**).

The electromagnetic waves at higher frequencies penetrate only near the surface of the conducting shield and the magnitude of the field exponentially decays with thickness. The distance (i.e., the thickness of the shield) required for the electromagnetic wave to be diminished to 1/e or 37% is known as the skin depth (δ), which can be mathematically expressed by Eq. 8 [**23**].

$$\delta = \sqrt{\frac{1}{\pi f \sigma \mu}} \qquad (4)$$

in which μ_r is the magnetic permeability, $\sigma = \omega\ \varepsilon_0 \varepsilon''$ is the AC conductivity and f is the frequency.

4.2 Determination of the Bandwidth Criterion of the Ras

Small thickness and a broad bandwith of RAs are important for the practical applications of RAs. The bandwidth of an RA at - 10 dB was calculated from the measured data as a function of the absorber thickness:

$$\frac{\Delta \lambda}{d} \qquad (5)$$

in which d is the total thickness of the absorber and $\Delta\lambda = \lambda_{max} - \lambda_{min}$.

5 Results and Discussion

5.1 Morphology of the Magnetic Fillers

The SEM images of the magnetic fillers used for preparing the composites are shown in **Fig. 3**. According to the SEM image (**Fig. 3**a), the CI particles are spherical and varying in size within a few microns in diameter, herewith a significant part of the particles form irregularly-shaped aggregates.

Polycrystalline particles of MnZn ferrite consist of separate grains in the form of polyhedrons with clear-cut boundaries (**Fig. 3**b). The total area of the interface between the grains reaches a significant value, which weakens the grain contacts in a composite and thus affects demagnetization [**15, 24**].

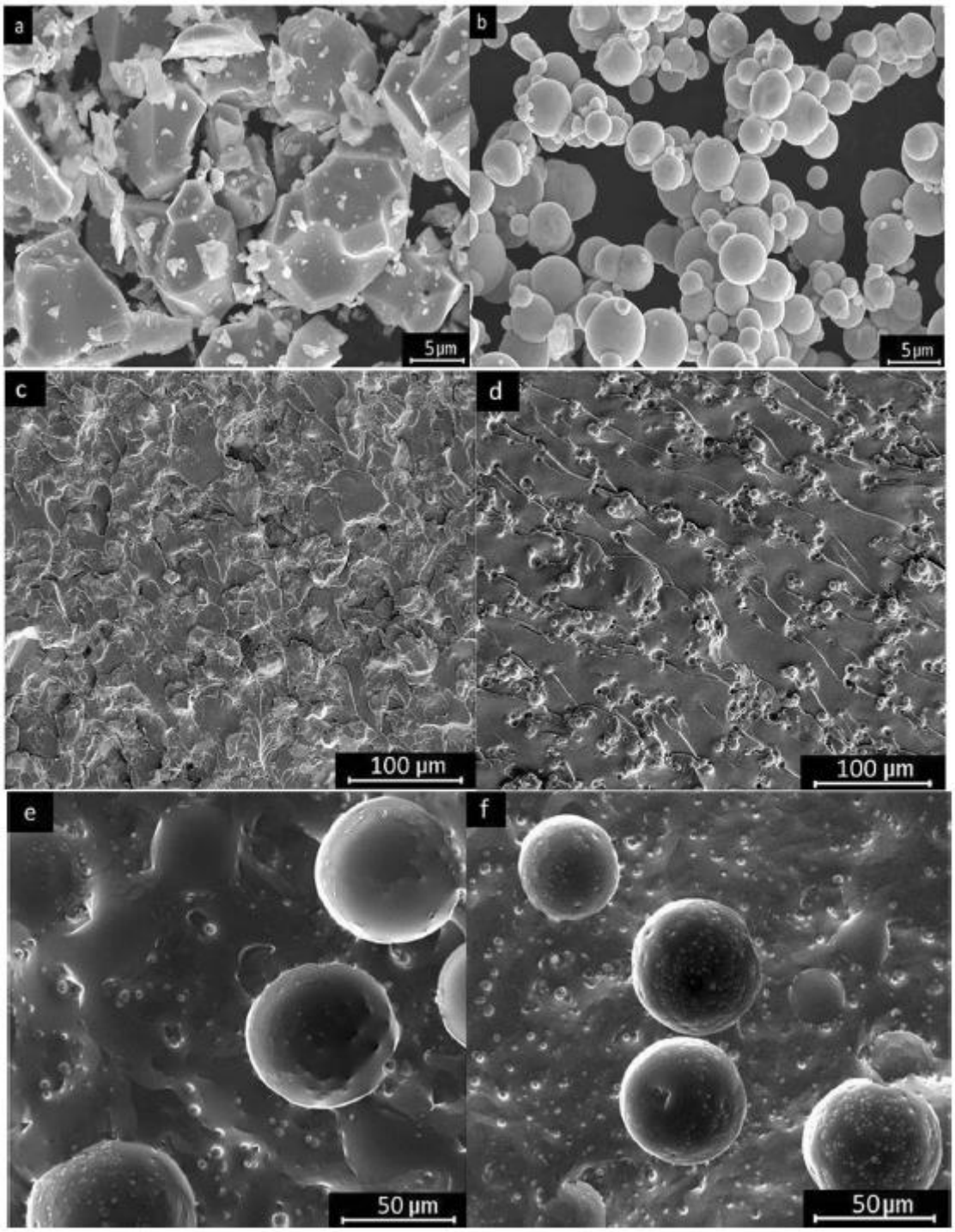

Fig. 3 The SEM micrographs of the magnetic filler: **a** MnZn ferrite **b** CI ferrite and the composites: **c** ER/MnZn50 **d** ER/ CI50 **e** ER/PDMS10/CI70 and f ER/PDMS10/CI80

5.2 Morphology of the Polymer Matrixes and the Magnetic Composites on their Base

The SEM images of the polymer matrixes and the magnetic composites on their base are shown in **Fig. 3**. The neat ER shows a smooth fracture surface at the brittle failure (**Fig. 3**c). The epoxy resin modified by PDMS (10-30 wt.%) exhibits a two-phase microstructure consisting of spherical elastomeric particles (15-90 μm) uniformly distributed in a bulk of the ER (**Fig. 3**e, f). From the ER-PDMS SEM images the presence of plastic shear deformation in composites is also visible, which can be identifed by the

presence of cracks propogating from the elastomer inclusions as stress concentrators. An increase in the filler content to 70-80 wt.% leads to the formation of particle clusters both in the bulk of the composite and at the ER-PDMS-interface (**Fig. 3**e, f).

5.3 Complex Permittivity Spectra of the Composites

The complex permittivity spectra of the composites are shown in **Fig. 4**. The composites with MnZn ferrite show a frequency dispersion of ε^* in the entire investigated frequency range, and it is more pronounced for the highly-filled composites. The ε' and ε'' values gradually increase with the filler content. The effect of the polymer matrix composition on the complex permittivity appeared for the composites with 70-80 wt.% of filler.

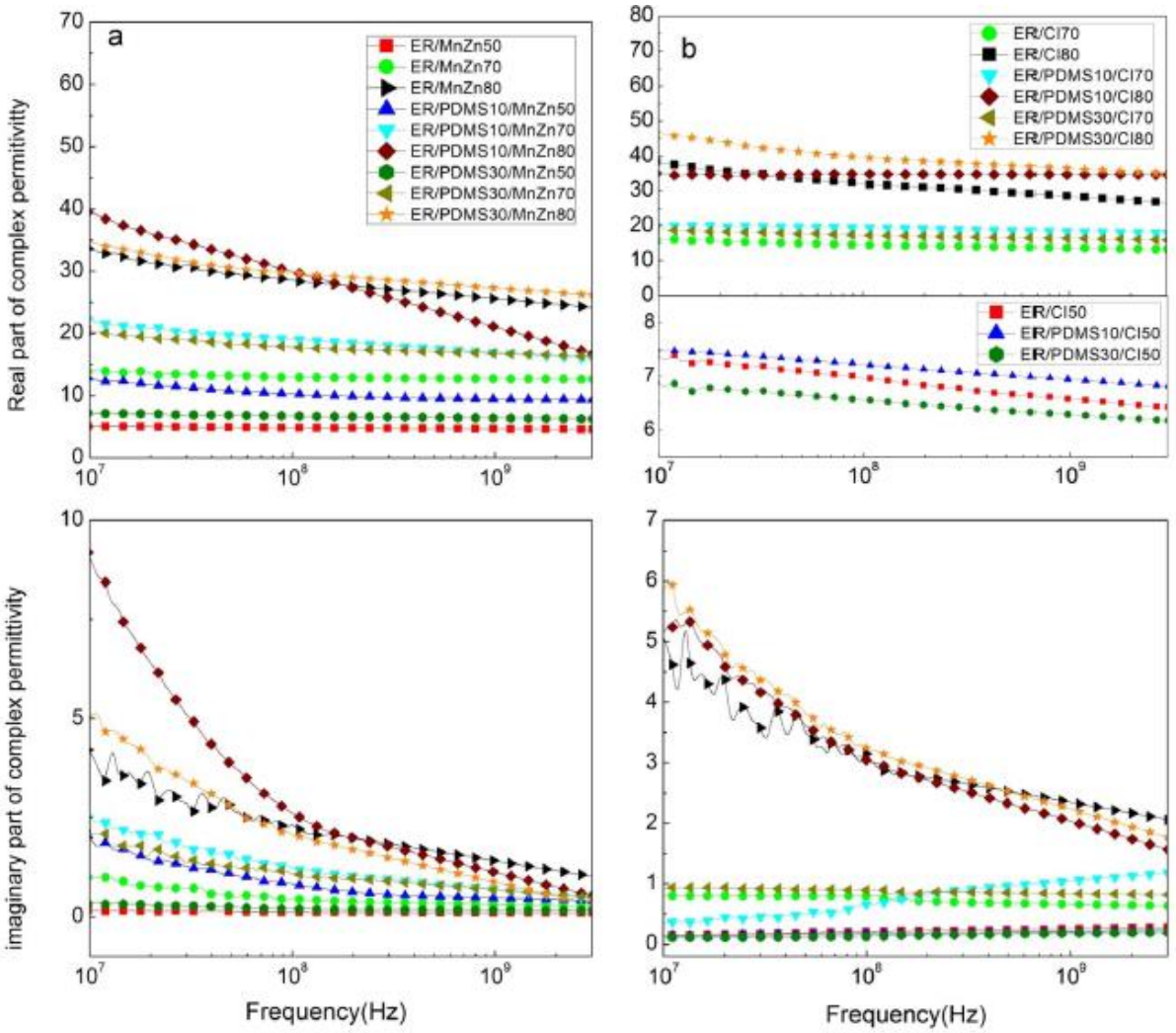

Fig. 4 The frequency dependences of the complex permittivity of the polymer composites filled with **a** MnZn and **b** CI (wt.%)

Thus, the ER/PDMS-MnZn composites show higher values of ε'and ε" compared with the ER composites with the same filler concentration. As to the composites with CI, the frequency dispersion of the complex permittivity is less pronounced compared to the composites with MnZn ferrite, but ε' and ε" are increasing with the filler concentration to approximately the same level as in the composites with MnZn ferrite. The polymer matrix composition affects ε' in the low RF region for the highly-filled CI-based composites, but it does not affect their dielectric losses. It seems that the permittivity spectra

of the composites caused by the electrical polarization induced in the filler particles and the particle clusters.

5.4 Complex Permeability Spectra of the Composites

It is well-known that magnetic properties of composites are related not only to the type and the concentration of the magnetic filler but also to the interaction among the magnetic particles through the polymer matrix [**25, 26**]. An obstruction to the interparticle interaction is the main reason for a lower value of μ^* in composites compared with that in bulk magnetic materials. The complex permeability spectra of the composites obtained are shown in **Fig. 5**.

The frequency dependence of the μ^* of the MnZn and CI based composites is determined first of all by the type of magnetic filler and its concentration. MnZn ferrite belongs to the spinel-type ferrites with nearly zero magnetocrystalline anisotropy and characterized by a single dispersion of magnetic spectra, which is associated with the superposition of a domain-wall resonance at about 10^6 Hz and a spin resonance at about 10^7 Hz [**27**]. Thus, the permeability dispersion region for the MnZn-based composites occupy a frequency range from 10^6 Hz up to 10^9 Hz, with a maximum value of μ' = 10 and μ'' = 3 for 80 wt.% of filler.

The CI-based composites demonstrate similar behavior of magnetic spectra with the difference that the ferromagnetic resonance linewidth is broader, 10^6—10^{10} Hz.

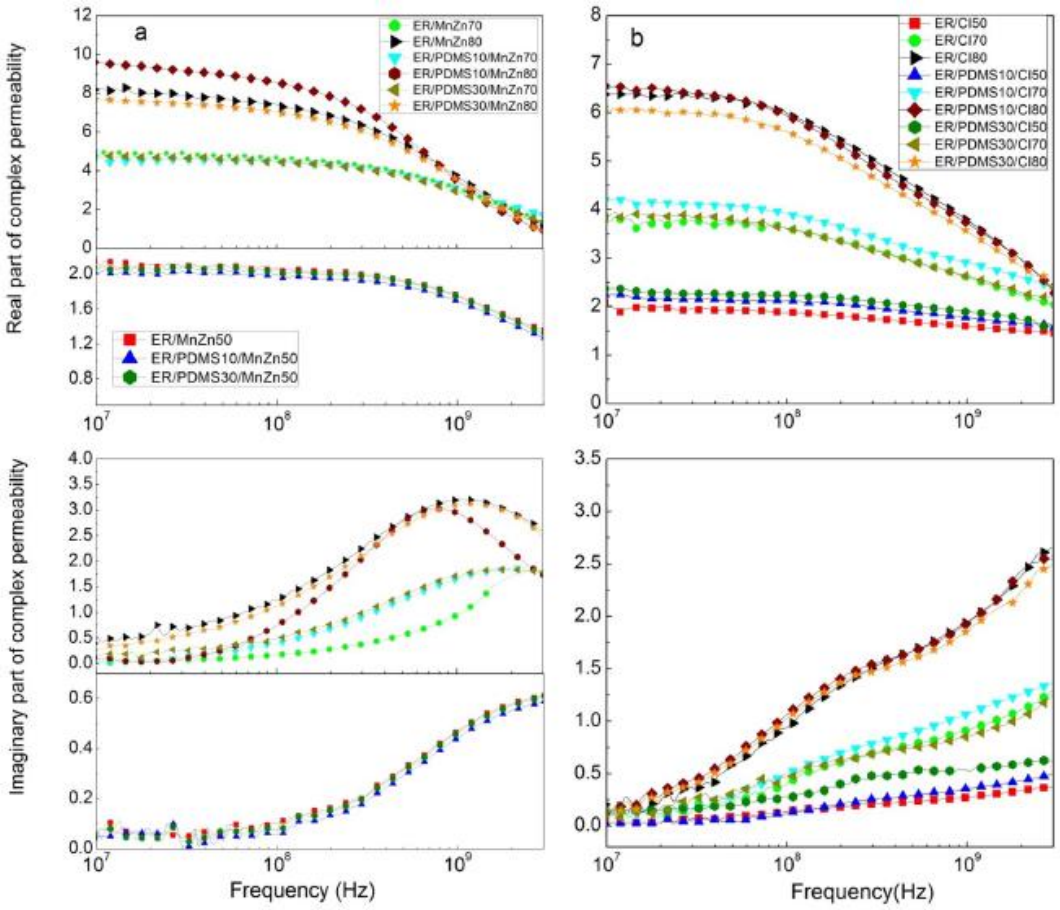

Fig. 5 The frequency dependence of the complex magnetic permeability of the polymer composites filled with **a** MnZn and **b** CI (wt.%)

However, the absolute value of the μ^* is lower compared to the composites filled with MnZn ferrite due to the skin effect which masks the magnetization processes in the conductive CI particles (**Fig. 6**). Besides, there are two peaks on μ"(f) for the composites with 50-80 wt.% of CI at about 108 Hz (domain-wall resonance) and 3 X 10^9 Hz (spin resonance) which can be explained by the complex micromagnetic structure of the SL type CI, exhibited polycrystalline structure [**19**]. The real and imaginary part of the μ^* in the composites increases with the concentration of the filler, regardless of the polymer matrix type. At the same time, there is a sharp increase in both components of μ^* with a filler concentration which indicates a gradual decrease in the internal demagnetizing field. The value of the demagnetizing field depends on the intrinsic properties of the filler, the shape and size of the magnetic particles, the particle volume fraction as well as on the interparticle interactions leading to the growth of clusters [**28**]. To quantify the intensity of the interparticle interactions in the composites, the reciprocity factor was introduced by J.L. Mattei and M- Le Floc'h [**29**]. It was found theoretically and experimentally that at a filler concentration exceeding 35 vol.%, reciprocity the factor is close to the maximum value, while the demagnetizing field approaches its minimum [**30**]. According to the magnetic spectra (**Fig. 5**), the demagnetizing field in the composites with all types of the polymer matrix approaches a minimum at 80 wt.% (45 vol.%) of MnZn and CI. The SEM images of the highly-filled composites indicate the formation of particle clusters as in the volume of the composite as on the ER/ PDMS interface (**Fig. 3**e, f).

As the particles make a chain, demagnetization decreases due to a decrease in the magnetic poles number and the formation of the continuity magnetization flux lines (**Fig. 7**).

5.5 Analysis of the Radio-Absorber Performance

In order to characterize the electromagnetic wave absorption properties of the composites obtained, the reflection minima of single-layer metal-backed absorbers was calculated within the layer thickness (**Eq. 3**). The results obtained are shown in **Figs. 8, 9** and **10**. After that, the operating absorption bandwidth at—10 dB level of RL was evaluated (Eq. 9) and shown in **Table 2**.

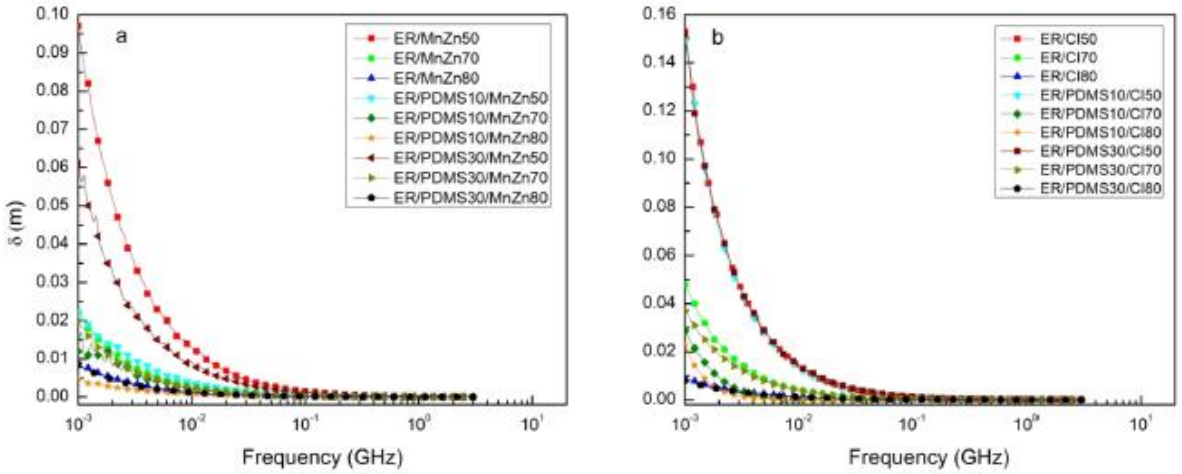

Fig. 6 The skin depth of the composites as a function of frequency **a** MnZn-based composites **b** CI-based composites

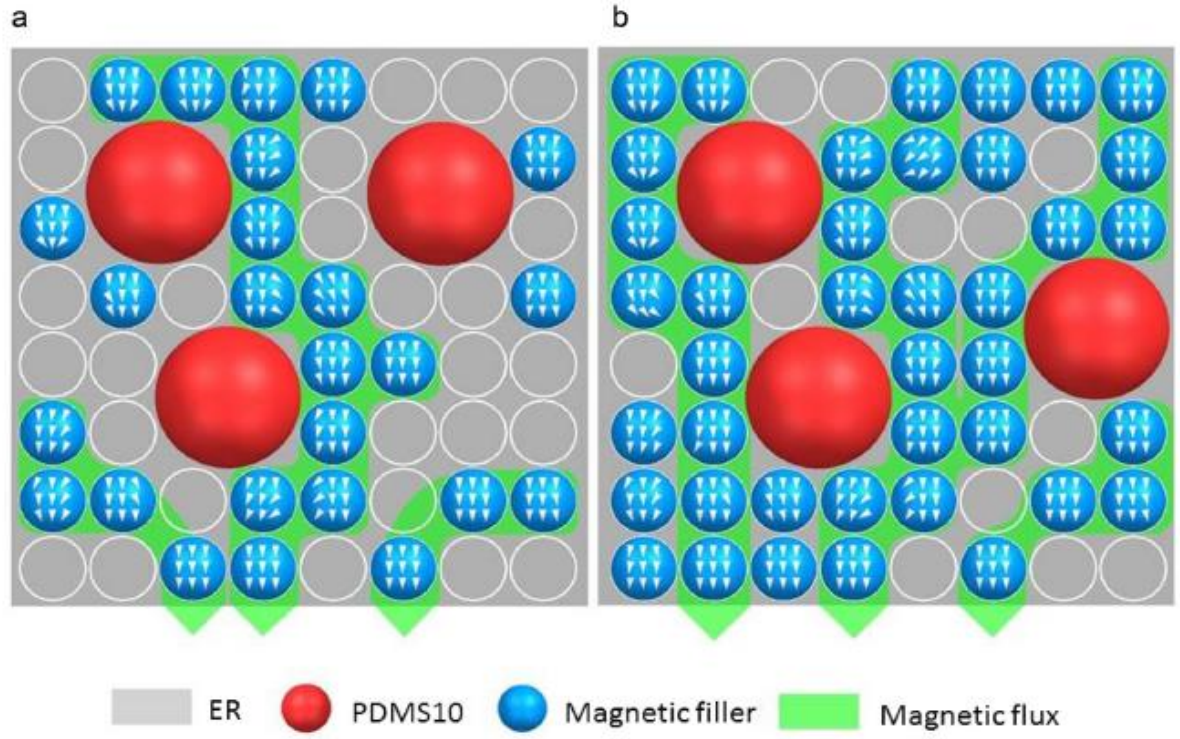

Fig. 7 Scheme of the filler concentration on internal demagnetizing field in the magnetic composites: a 50 wt.% magnetic filler b 70 wt.% magnetic filler

As can be seen, the type and concentration of the magnetic filler in the composite, as well as its thickness, make it possible to achieve a matching condition of absorber at a certain frequency of the radio-frequency band. In addition to the above, the matching frequency shifts to the low-frequency region with an increase in filler concentration. It can be explained by an increase in the effective value of the dielectric constant. In this case, the wavelength is shortened as $\lambda_m = \lambda/\sqrt{\varepsilon\mu}$ and the resonance thickness is equal to $\lambda/4$. Thus, for the same thickness of the absorber layer, the resonant wavelength of the absorber is greater, the greater the dielectric constant. Simultaneously, the bandwidth to thickness ratio of the absorber depends mostly on the filler type. The composites with MnZn ferrite demonstrate a larger bandwidth to thikness ratio in comparison with the CI filled composites due to a proper ratio between ε^* and μ^* which leads to the impedance matching conditions between the RAs and the free space.

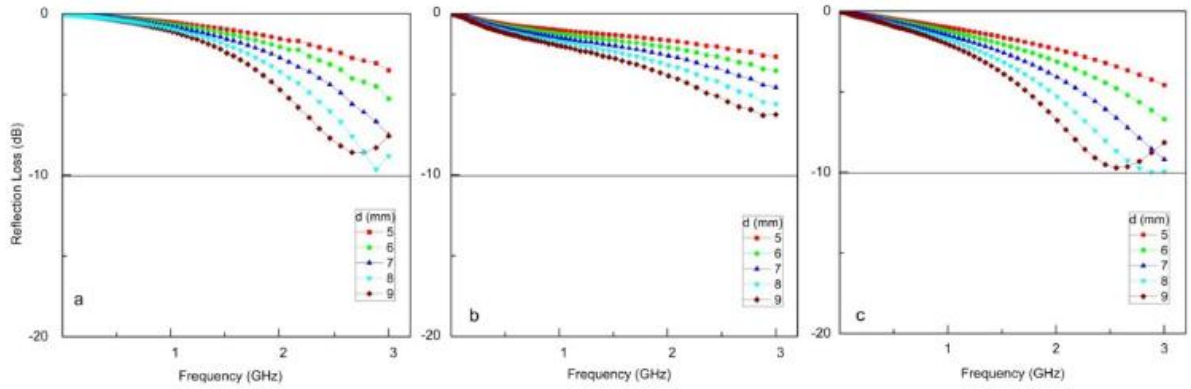

Fig. 8 The frequency dependence of the reflection loss of the composites filled with 50 wt.% CI based on: **a** ER **b** ER/PDMS10 and **c** ER/ PDMS30

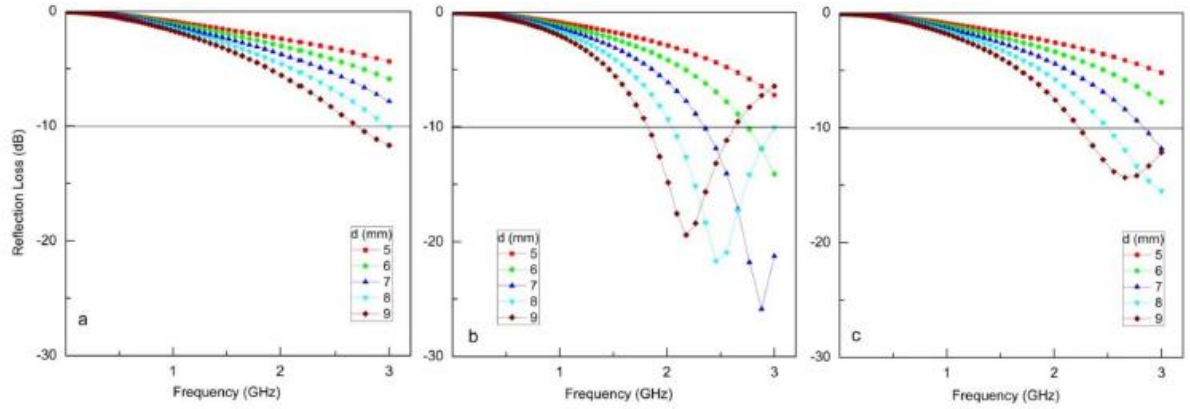

Fig. 9 The frequency dependence of the reflection loss of the composites filled with 50 wt.% MnZn based on: **a** ER **b** ER/PDMS10 and **c** ER/ PDMS30

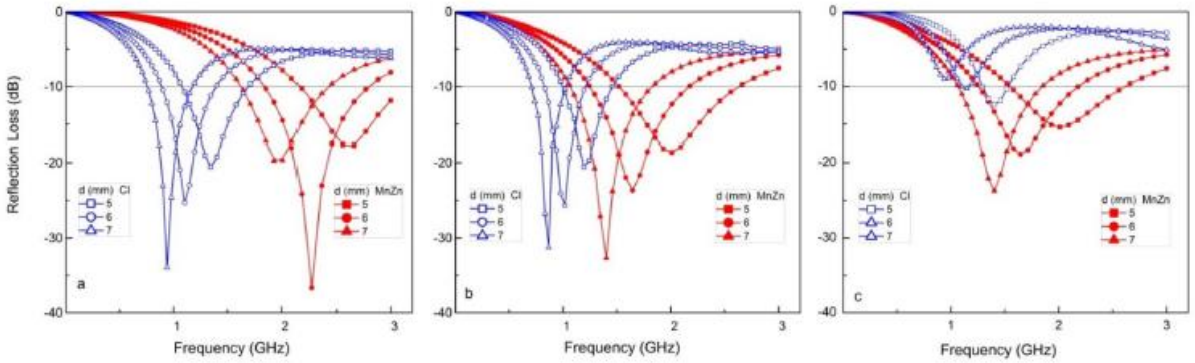

Fig. 10 The frequency dependences of the reflection loss of the composites filled with MnZn (36 vol.% = 70 wt.%) and CI (36 vol.% = 80 wt**.%)** based on: **a** ER **b** ER/PDMS10 and **c** ER/PDMS30

Table 2 The operating absorption bandwidth at -10 dB level of RL for the absorbers based on different composites

Composites	$\Delta\lambda/d$ (at the level of −10 dB) d (mm)					
	5	6	7	8	9	10
ER/MnZn50	–	–	–	–	–	–
ER/MnZn70	7.60	9.15	8.30	7.48	3.68	–
ER/MnZn80	28.50	29.67	28.27	29.69	28.40	26.8
ER/PDMS10/MnZn50	6.6	6.3	6.28	5.81	5.64	5.24
ER/PDMS10/MnZn70	15.84	16.38	16.33	16.19	14.96	13.46
ER/PDMS10/MnZn80	35.88	38.23	38.10	38.35	42.48	35.21
ER/PDMS30/MnZn50	6.48	5.88	5.35	5.37	4.46	4.14
ER/PDMS30/MnZn70	15.44	16.60	16.90	16.68	16.06	15.03
ER/PDMS30/MnZn80	25.18	27.93	26.59	28.29	24.87	23.89
ER/CI50	0.92	0.78	0.94	–	–	–
ER/CI70	9.40	10.03	9.67	9.31	8.37	8.02
ER/CI80	19.94	19.78	19.94	20.15	19.47	18.83
ER/PDMS10/CI50	0.96	0.98	0.9	–	–	–
ER/PDMS10/CI70	12.16	11.82	11.01	11.29	9.47	9.44
ER/PDMS10/CI80	17.56	18.78	18.70	18.23	19.50	17.15
ER/PDMS30/CI50	0.54	0.86	0.9	0.61	–	–
ER/PDMS30/CI70	9.52	9.57	8.97	9.14	8.21	7.84
ER/PDMS30/CI80	6.80	2.68	–	–	–	–

It is also necessary to emphasize the effect of the polymer matrix on the radio-absorber performance of the magnetic composites. In general, it can be found that the magnetic composites based on the ER/PDMS10 matrix achieved higher RL bandwidths than the ER and the ER/PDMS30 composites with the same magnetic filler content (**Table 2**), which is in accordance with the dielectric and the magnetic spectra (**Figs. 4, 5**).

Figure 8 depictes the RL of the composites based on the ER and the ER blends with 10 and 30 wt.% of PDMS and 50 wt.% of CI. Such a high concentration of CI in the polymer matrix leads to the RL varying from - 5 dB to - 10 dB, which is due to the low skin depth which masks the magnetization processes in the conductive CI particles as discussed previously. However, there is tendency that with increasing the PDMS concentration up to 30 wt.%, the value of the RL increases and the RL minimum shifts to a higher frequency range which is more probably related to clustering and the localization of the conductive CI particles at the ER-PDMS interface as discussed in study of percolation threshold [**18**].

Figure 9 shows the RL dependence for the composites with 50 wt. % of MnZn-ferrite in the ER matrix and blends with a different PDMS content. The composite ER/MnZn50 demonstrates an RL of about -10 dB within a bandwith ($\Delta\lambda$/d = 2.21) for 11 mm RA thickness and ($\Delta\lambda$/d = 1.35) for 12 mm RA thickness. The addition of 10 wt.% of PDMS to the ER (ER/PDMS10/MnZn50) results in a higher absorption (-25 dB) within a broader bandwith (AX/d = 6.28) for an RA with a thickness of about 7 mm. However, an increase in the PDMS up to 30 wt.% leads to a lower RL (-18.5 dB) and a narrow bandwith ($\Delta\lambda$/d = 5.35).

An increase in the filler concentration up to 70 wt.% (36 vol.%) provides 99% of the electromagnetic energy absorption (**Fig. 10**). Besides that, the magnetic composites with a different PDMS content in the ER matrix exibit a different operating frequency range: for the MnZn-filled composites Δf = 1.6-3 GHz, while for the CI- filled composites Δf = 0.7-1.7 GHz. According to the results obtained, the presence of 10 wt.% PDMS in both types of composites is sufficient to reduce the demagnetization effect and to obtain broadband RAs with a thickness of 5-7 mm.

5.6 DMA Analysis

According of the results obtained (**Fig. 11**a), the ER exhibits a storage modulus of about 4300 MPa; however, around - 40 °C, there is a first decrease up to 2600 MPa, which corresponds to the movement of the side groups of the polymer chain (y-relaxation) (**Fig. 11**a).

A significant temperature drop of E' at 140 °C more probably related to the segmental motion of the polymer chains (a-relaxation) in the ERs. Typically, as the temperature approaches the T_g, the storage modulus markedly drops (**Table 3**). The T_g was determined from the maximum value of the tan δ peak and it decreases for polymer blends with an increase to the PDMS content from 10 to 30 wt.% (**Fig. 11**b).

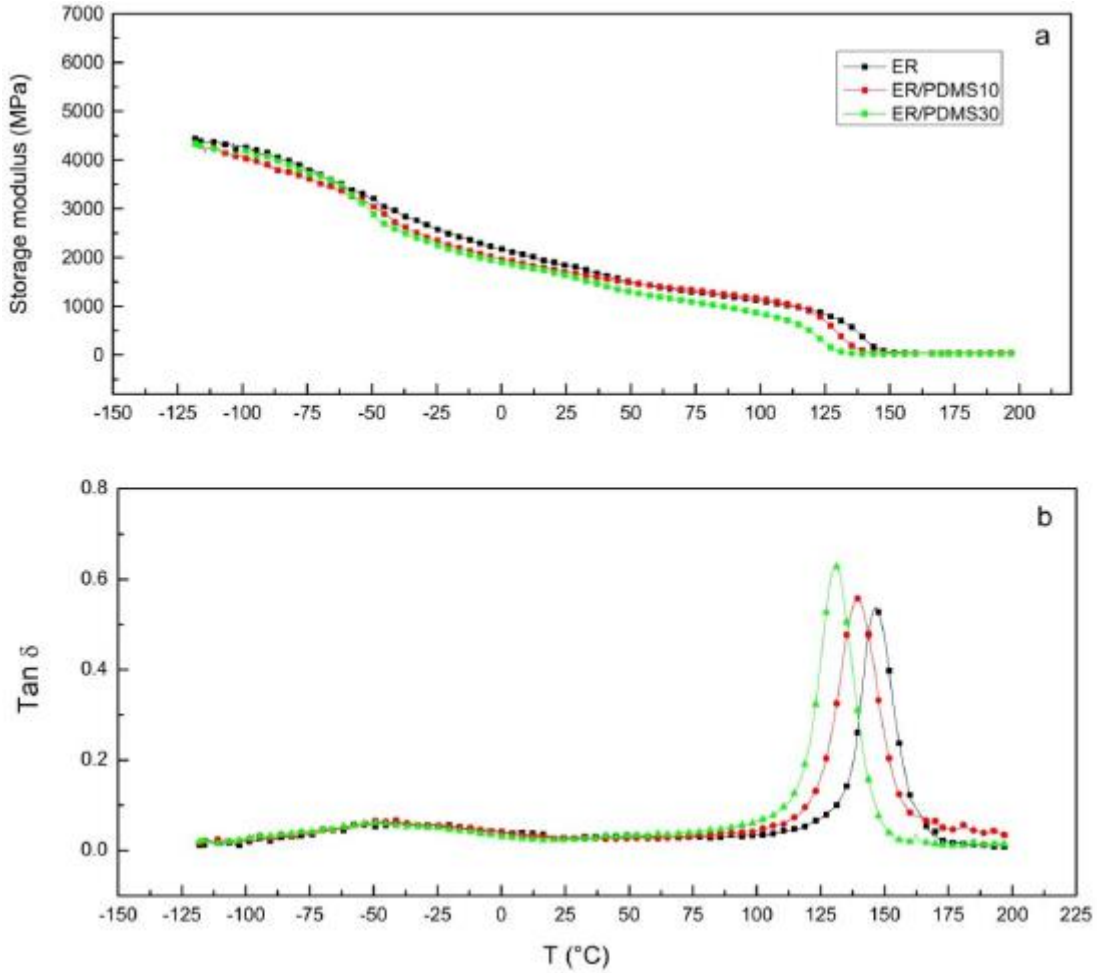

Fig. 11 The temperature dependences of **a** the storage modulus E' and **b** tan 5 of pure ER, PDMS10 and PDMS30

The polymer blend of neat epoxy resin (ER) and PDMS was studied previously in [**17**]. **Figures 12** and **13** show the DMA curves of the magnetic composites filled with MnZn and CI. The storage modulus (E') of the composites increases with increses in the filler concentraion from 50 up to 70 wt.% due to high Young's modulus of filler (MnZn ~ 124 GPa; CI ~ 207 GPa), which is in an agreement with the mixing rule.

However, Young's modulus of composites decreased at 80 wt.% of the filler which attributed to the lowering of the cross-linking density due to high-particles content in the polymer matrix (**Figs. 12**a, **13**a).

The effect of interfacial interactions on the dynamic mechanical properties of the filled polymers depends on several factors [**31**]. These factors include the physical properties of the fillers (particle size, surface area, particle size distribution, geometry of the particles, etc.), the quality of filler dispersion in the matrix and the concentration of the filler in the composite. Most of the studies [**6, 9**] suggested that in the event of a strong interfacial interaction between the matrix and the filler, the peak value of tan δ reduces, whereas T_g of the composite increases. In our study, we did not find a visible change in T_g for the composites filled with MnZn ferrite, but for a composite with CI, T_g decreases due to the filler oxidation processes, which was confirmed by the results of the XPS (**Fig. 13**c).

Table 3 The values of E' and T_g of the composites as a function of the temperature

Composites	E′(MPa) 80 °C	E′ (MPa) 40 °C	Tan δ	T_g (°C)
ER	4005	1677	0.53	146
ER/PDMS10	3688	1571	0.56	139
ER/PDMS30	3880	1508	0.63	130
ER/PDMS10/ MnZn50	2646	888	0.84	127
ER/PDMS10/ MnZn70	3300	2134	0.54	130
ER/PDMS10/ MnZn80	3950	2588	0.33	132
ER/PDMS30/ MnZn50	2988	1342	0.65	130
ER/PDMS30/ MnZn70	4319	2419	0.54	132
ER/PDMS30/ MnZn80	4634	2673	0.33	127
ER/PDMS10/CI50	3354	2225	0.92	135
ER/PDMS10/CI70	4631	3205	0.65	140
ER/PDMS10/CI80	5461	4005	0.42	139
ER/PDMS30/CI50	4631	2640	0.88	130
ER/PDMS30/CI70	6411	3649	0.61	118
ER/PDMS30/CI80	6174	2819	0.27	118

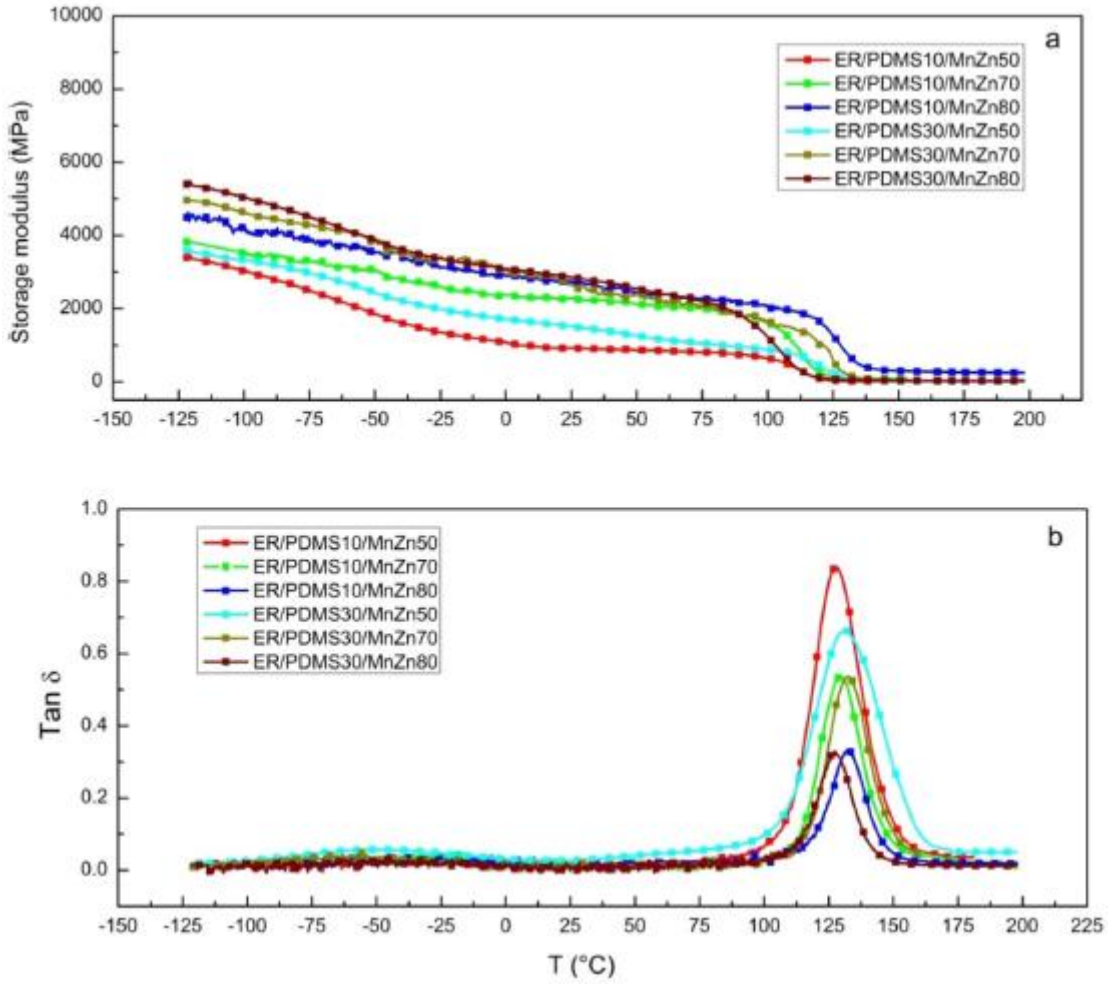

Fig. 12 The temperature dependences of **a** the storage modulus E' and **b** tan δ of composite filled by MnZn

It can be seen that the ER/PDMS sample with a low concetration of corroded CI exhibited higher tanδ conditions as indicated by an increase in the T_g. It is noted here that the oxidation layer which appeared on the corroded CI was mostly brittle and might lead to changes to its material properties, such as the tanδ and T_g [**32**]. Besides that, with increasing the content of the PDMS in the composites cured by DCP, the T_g significantly decreases.

Figures 12b, **13**b show that when the particle size of the filler remains constant, increasing the amount of the filler results in: (i) a decrease in the peak tan δ, (ii) a slight increase in T_g, and (iii) a large increase in the storage modulus. This indicates that the role of the interaction at the filler—polymer interface.

5.7 Charpy Impact Strength

The variation of the impact strength with MnZn and CI content for the composite is shown in **Fig. 14**.

Incorporating a magnetic filler and PDMS into the epoxy resin enhances the composites toughness (**Table 1**). The addition of 50 wt.% of MnZn or CI has a similar effect on the impact strength as addition of 10-30 wt.% of PDMS, which is about 17 kJ/m^2 [**17**]. A further increase in the filler or the PDMS content leads to a gradual decrease in the impact strength. The values of the impact strength for the composites with 50 wt.% of magnetic filler with 10 or 30 wt.% of PDMS are about 15 kJ/m^2. The polymer composites with a high filler concentration increase the likelihood of particle agglomeration generating defects which initiates failure. A high filler content can also contribute to debonding at the elastomer-matrix interface, which can lead to crack propagation across the elastomer interface. The samples with the highest values of impact strength contained 50-70 wt.% of filler. There is no significant differencies among the composites with a different PDMS content, i.e. 10 or 30 wt.%. Generally, the size and the shape of the filler play an important role in the impact strength of composites. Composites with rough bigger MnZn particles are more brittle than composites with smaller spherical CI particles due to crack formation during loading.

6 Conclusion

A dual-phase polymer matrix (ER and PDMS) filled with MnZn-ferrite and CI was investigated with the aim to optimizing the electromagnetic properties of the composites in the RF range, as well as their mechanical properties. To meet this goal, the concentration of PDMS was varied from 10 to 30 wt.% which affects the distribution of the magnetic particles in the polymer matrix leading to locally-increased filler concentration in the ER phase.

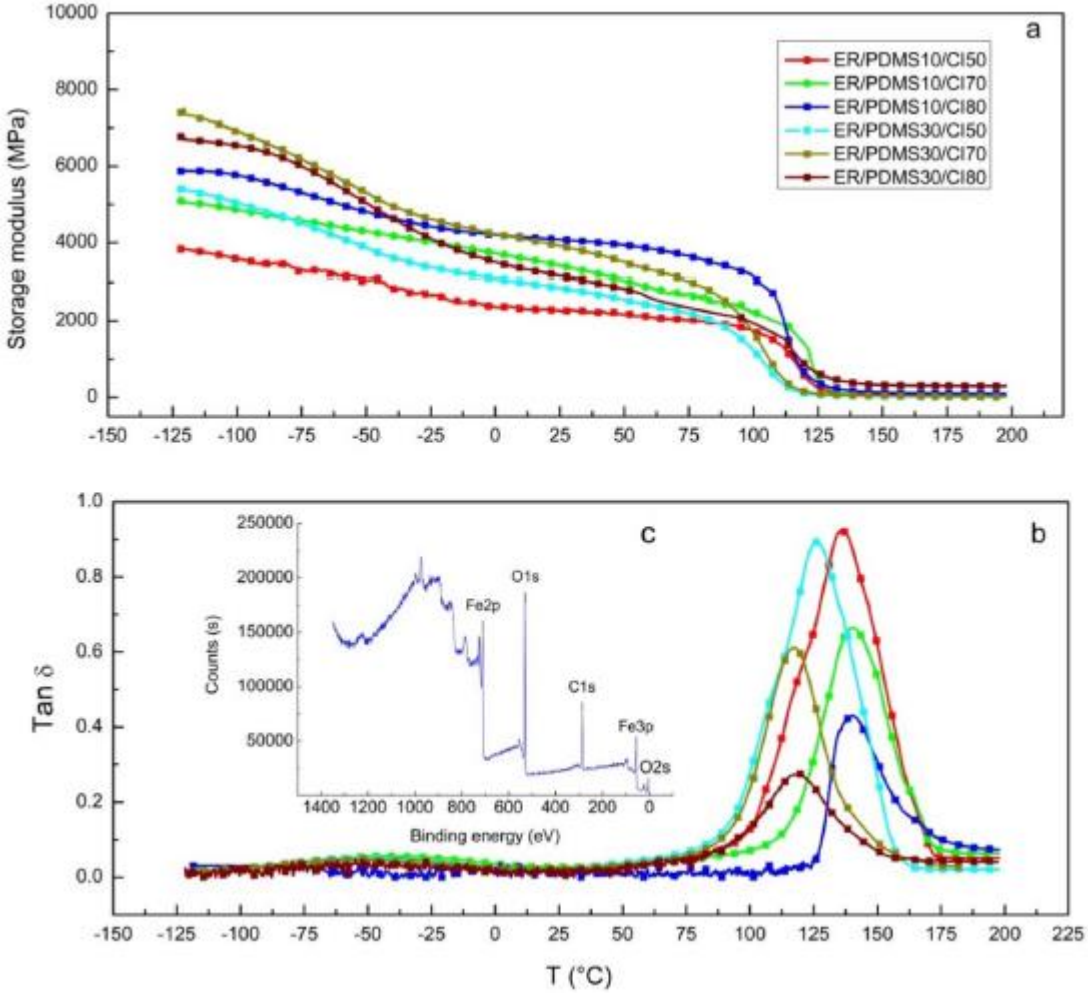

Fig. 13 The temperature dependences of **a** the storage modulus E' **b** tan δ of the composite filled by CI and **c** XPS of the ER/PDMS10/CI80

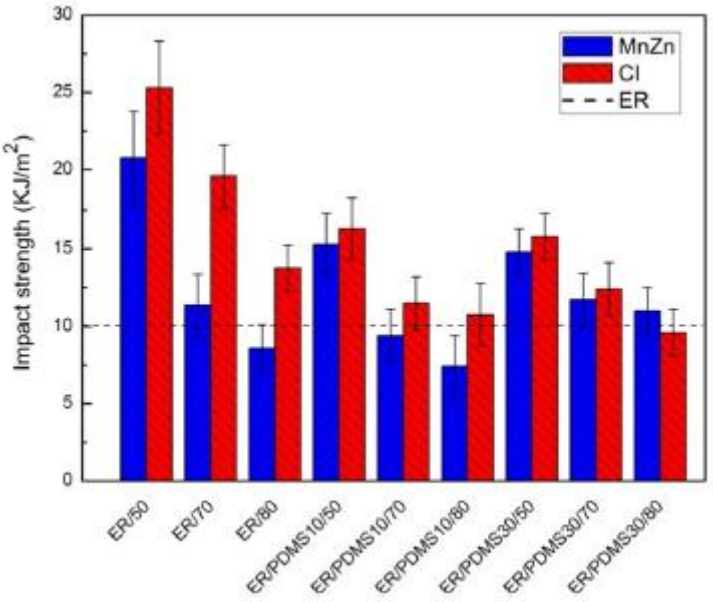

Fig. 14 The Impact strength of the magnetic composites filled by MnZn and CI

The SEM results showed that the filler is localized inside the ER phase and at the ER-PDMS-interface with good homogeneity. According to the dielectric and magnetic spectra, measured by the impedance method, the magnetic filler concentration and the polymer matrix composition affect the electromagnetic properties of composites, i.e. with increases in the filler and the PDMS content both complex permittivity and complex permeability increases. Based on the results obtained, the reflection minima of single-layer metal-backed absorbers was calculated within the layer thickness and then the operating absorption bandwidth at - 10 dB level of RL was evaluated. An analysis of the results obtained showed that the position of the RL minima moves to a lower frequency and the loss factors of the composites increase with increasing the filler concentration. It has been shown that, via a selection of the matrix (ER, ER/PDMS), it is possible to change the distribution of the filler thereby significantly lowering the reflection loss.

Overall, the presence of 10 wt.% PDMS in both types of composites is sufficient to reduce the demagnetization effect and to obtain broadband RAs with a thickness of 5-7 mm.

References

1. Meena, R.S., Bhattachrya, S., Chatterjee, R.: Complex permittivity, permeability and microwave absorbing properties of (Mn2xZnx)U-type hexaferrite. J. Magn. Magn. Mater. **322**, 29082914 (2010). **https://doi.org/10.1016/j.jmmm.2010.05.004**

2. Xie, S., Zhu, L., Zhang, Y., Ji, Z., Wang, J.: Three dimensional periodic structured absorber for broadband electromagnetic radiation absorption. Electron. Mater. Lett. **16**, 340-346 (2020). **https:// doi.org/10.1007/s 13391 -020-00219-y**

3. Zhou, Y., Li, W., Li, L., Sun, Z., Jiang, L., Ma, J., Chen, S., Ning, X., Zhou, F.L.: Lightweight and highly conductive silver nanoparticles functionalized meta-aramid nonwoven fabric for enhanced electromagnetic interference shielding. J. Mater. Sci. **56**, 64996513 (2021). **https://doi.org/10.1007/s10853-020-05600-8**

4. Stergioul, C.A., Koledintseva, M.Y., Rozanov, K.N.: Hybrid polymer composites for electromagnetic absorption in electronic industry. Hybrid Polym. Compos. Mater.: Appl. (2017). **https:// doi.org/10.1016/B978-0-08-100785-3.00003-6**

5. Naseer, A., Mumtaz, M., Raffi, M., Ahmad, I., Khan, S.D., Sha-koor, R.I., Shahzada, S.: Reinforcement of electromagnetic wave absorption characteristics in PVDF-PMMA nanocomposite by intercalation of carbon nanofibers. Electron. Matter. Lett. **15**, 201-207 (2019). **https://doi.org/10.1007/s13391-018-00104-9**

6. Rozanov, K.: Ultimate thickness to bandwidth ratio of radar absorbers. IEEE T. Antenn. Propag. 48(8), 1230-1234 (2000). **https://doi.org/10.1109/8.884491**

7. Microwave absorbing materials. Laird technologies. **http://www. lairdtech.com**

8. Ferrite absorbers. TDK RF Solutions Inc. **http://www.tdkrfsolut ions.com**

9. Vovchenko, L.L., Lozitsky, O.V., Matzui, L.Y., et al.: Microwave shielding and absorbing properties of single- and multilayered structures based on two-phase filler/epoxy composites. Appl. Nanosci. (2021). **https://doi.org/10.1007/s13204-021-01765-z**

10. Perigo, E.A., et al.: Past, present, and future of soft magnetic composites. J. Appl. Phys. Rev. **5**, 031301 (2018). **https://doi.org/10. 1063/1.5027045**

11. Sista, K.S., Dwarapudi, S., Kumar, D., Sinha, G.R., Moon, A.P.: Carbonyl iron powders as absorption material for microwave interference shielding: a review. J. Alloy. Compd. (2021). **https://doi. org/10.1016/j.jallcom.2020.157251**

12. Singh Yadav, R., Kuřitka, I., Vilčáková, J.: Advanced Spinel Ferrite Nanocomposites for Electromagnetic Interference Shielding Applications. Elsevier Inc., Netherlands (2020)

13. Batel, L., Mattei, J.L., Chevalier, A.: Tunable magneto-dielectric material for electrically small and reconfigurable antenna systems at vhf band. Ceramics **3**(3), 276-286 (2020). **https://doi.org/10. 3390/ceramics3030025**

14. Chevalier, A., Le Floc'h, M.: Dynamic permeability in soft magnetic composite materials. J. Appl. Phys. **90**, 3462-3465 (2001). **https://doi.org/10.1063/1.1389520**

15. Lopatin, A.V., Kazantseva, N.E., Kazantsev, Y.N., et al.: The efficiency of application of magnetic polymer composites as radioabsorbing materials. J. Commun. Technol. Electron. **53**, 487-496 (2008). **https://doi.org/10.1134/S106422690805001X**

16. Babayan, V., Kazantseva, N.E., Moučka, R., Sapurina, I., Spi-vak, Y.M., Moshnikov, V.A.: Combined effect of demagnetizing field and induced magnetic anisotropy on the magnetic properties of MnZn ferrite composites. J. Magn. Magn. Mater. **324**, 161-172 (2012). **https://doi.org/10.1016/j.jmmm.2011.08.002**

17. Vilčáková, J., Kutějová, L., Jurča, M., Moučka, R., Vícha, R., Sedlačík, M., Kovalcik, A., Machovský, M., Kazantseva, N.E.: Enhanced Charpy impact strength of epoxy resin modified with vinyl-terminated polydimethylsiloxane. J. Appl. Polym. Sci. **135**, 45720 (2018). **https://doi.org/10.1002/app.45720**

18. Jurča, M., Vilčáková, J., et al.: Reduced percolation threshold of conductive adhesive through nonuniform filler localization: monte Carlo simulation and experimental study. Compos. Sci. Technol. **214**, 108964 (2021). **https://doi.org/10.1016/).comps citech.2021.108964**

19. Abshinova, M.A., Lopatin, A.V., Kazantseva, N.E., Vilčáková, J., Sáha, P.: Correlation between the microstructure and the electromagnetic properties of carbonyl iron filled polymer composite. Compos. Part A-Appl. S. **38**, 2471-2485 (2007). **https:// doi.org/10.1016/j.compositesa.2007.08.002**

20. Moučka, R., Lopatin, A.V., Kazantseva, N.E., et al.: Enhancement of magnetic losses in hybrid polymer composites with MnZn-ferrite and conductive fillers. J Mater Sci **42**, 9480-9490 (2007). **https ://doi.org/10.1007/s 10853-007-2081 -0**

21. Pauw, L.: A method of measuring specific resistivity and Hall effect of discs of arbitrary shape. Philips Res. Rep. **13**(1), 1-9 (1958). **https://doi.org/10.1142/9789814503464_0017**

22. Ge, Y., Li, C., Waterhouse, G.I.N., et al.: ZnFe2O4@PDA@ Polypyrrole composites with efficient electromagnetic wave absorption properties in the 18-40 GHz region. J. Mater. Sci. **56**, 10876-10891 (2021). **https://doi.org/10.1007/ s10853-021-05968-1**

23. Sankaran, S., Deshmukh, K., Ahamed, M.B., Pasha, S.K.K.: Recent advances in electromagnetic interference shielding properties of metal and carbon filler reinforced flexible polymer

composites: a review. Compos. Part A-Appl. S. **114**, 49-71 (2018). **https://doi.org/10.1016/j.compositesa.2018.08.006**

24. Mattei, J.L., Le Floc'h, M.: A numerical approach of the inner demagnetizing effects in soft magnetic composites. J. Magn. Magn. Mater. **215-216**, 589-591 (2000). **https://doi.org/10. 1016/S0304-88 53(00)00230-4**

25. Kong, L.B., Li, Z.W., Liu, L., Huang, R., Abshinova, M., Yang, Z.H., et al.: Recent progress in some composite materials and structures for specific electromagnetic applications. Int. Mater. Rev. **58**, 203-259 (2013). **https://doi.org/10.1179/1743280412Y. 0000000011**

26. Lagarkov, A.N., Rozanov, K.N.: High-frequency behaviour of magnetic composites. J. Magn. Magn. Mater. **321**, 2082-2092 (2009). **https://doi.org/10.1016/j.jmmm.2008.08.099**

27. Tsutaoka, T.: Frequency dispersion of complex permeability in Mn-Zn and Ni-Zn spinel ferrites and their composite materials. J. Appl. Phys. **93**, 2789-2796 (2003). **https://doi.org/10.1063Z1. 1542651**

28. Moore, R.L.: Development and test of concentration scalled demagnetization in effective media theories of magnetic composites. J. Appl. Phys. **125**, 085101 (2019). **https://doi.org/10. 1063/1.5053791**

29. Mattei, J.L., Le Floc'h, M.: Effects of the magnetic dilution of the ferromagnetic resonance of disordered heterostructures. J. Magn. Magn. Mater. **264**, 86-94 (2003). **https://doi.org/10. 1016/S0304-88 53(03)00143-4**

30. Mattei, J.L., Le Floc'h, M.: Percolative behavior and demagnetizing effects in disordered heterostructures. J. Magn. Magn. Mater. **257**, 335-345 (2003). **https://doi.org/10.1016/S0304-8853(02)01232-5**

31. Huang, Y., Song, W.-L., Wang, Ch., Xu, Y., Wei, W., Chen, M., Tang, L., Fang, D.: Multi-scale design of electromagnetic composite metamaterials for broadband microwave absorption. Compos. Sci. Technol **162**, 206-214 (2018). **https://doi.org/10.1016/)'. compscitech.2018.04.028**

32. Abdul Aziz, S.A.B., Mazlan, S.A., Nordin, N.A., Abd Rahman, N.A.N., Ubaidillah, U., Choi, S.B., Mohamad, N.: Material characterization of magnetorheological elastomers with corroded carbonyl iron particles: morphological images and field-dependent viscoelastic properties. Int. J. Mol. Sci. **20**(13), 3311 (2019). **https ://doi.org/10.3 390/ij ms20133311**